A&A 401, 903–910 (2003)
DOI: 10.1051/0004-6361:20030160

Astronomy & Astrophysics

The history of the iron K_α line profile in the Piccinotti AGN ESO 198-G24

M. Guainazzi

XMM-Newton Science Operation Center, VILSPA, ESA, Apartado 50727, 28080 Madrid, Spain

Received 26 August 2002 / Accepted 30 January 2003

Abstract. This paper presents ASCA (July 1997), XMM-Newton (December 2000) and BeppoSAX (January 2001) observations of the Piccinotti Seyfert 1 galaxy ESO 198-G24. The BeppoSAX 0.1–200 keV spectrum exhibits reprocessing features, probably produced by an X-ray illuminated, relativistic accretion disk subtending a solid angle $\lesssim 2\pi$. During the XMM-Newton observation the fluorescent iron K_α line profile (centroid energy $E_c \simeq 6.4$ keV) was broad and twice as bright as in the BeppoSAX observation. An additional emission feature ($E_c \simeq 5.7$ keV), detected at the 96.3% confidence level, may be part of a relativistic, double-peaked profile. By contrast, in the earlier ASCA observation the line profile is dominated by a remarkably narrow "core" (intrinsic width, $\sigma < 50$ eV). If this component is produced by reflection off the inner surface of a molecular torus, its large Equivalent Width ($\simeq$300 eV) most likely represents the "echo" of a previously brighter flux state, in agreement with the dynamical range covered by the historical X-ray light curve in ESO 198-G24.

Key words. accretion, accretion discs – galaxies: active – galaxies: individual: ESO 198-G24 – X-rays: galaxies – galaxies – nuclei

1. Introduction

The discovery of the broadened and skewed fluorescent iron K_α line profile in the first "long-look" ASCA observation of MCG-6-30-15 (Tanaka et al. 1995) fostered the hope that general relativistic effects could be observationally studied through X-ray spectroscopy of nearby Active Galactic Nuclei (AGN). This hope was further strengthened by the discovery that about 50% of the known bright Seyfert 1s exhibit broad line profiles (Nandra et al. 1997). It was reasonable to expect that the advent of *Chandra* and XMM-Newton would allow to significantly extend the depth and range of these studies.

These hopes are now facing a complex reality. In a few objects the existence of a relativistically broadened iron line profile is out of question (Nandra et al. 1999; Wilms et al. 2001; Turner et al. 2002; Fabian et al. 2002). However, often the observed profiles do not match the theoretical calculations (Fabian et al. 1989; Laor 1991; Matt et al. 1992). Electron scattering, as often observed in type 2 Seyferts (Ueno et al. 1994; Turner et al. 1997; Matt et al. 2000), may help reconciling the difference between observed and theoretical line profiles produced in X-ray illuminated, relativistic accretion disks (Reeves et al. 2001; Matt et al. 2001). Other pieces of evidence suggest constraints on the nature of the accretion: the disk may be truncated at a radius where relativistically broadened wings are negligible (see, e.g. the discussion in O'Brien et al. 2001), or may develop a hot "skin" (Nayakshin et al. 2000; Ballantyne et al. 2001), which may contribute to the iron line profile through transitions of highly ionized stages. Observations with the *Chandra* high-energy gratings (Yaqoob et al. 2001; Kaspi et al. 2002; Weaver 2001, and references therein) and with XMM-Newton (Gondoin et al. 2001a,b; Pounds et al. 2001; Petrucci et al. 2002) have often unveiled narrow line components. When measured at the currently highest possible energy resolution, their intrinsic velocities are consistent with the width of the optical broad lines, suggesting an origin in the same medium. However, different origins (e.g. scattering off the inner side of the molecular "torus" envisaged by the Seyfert unification scenarios; Antonucci & Miller 1985; Antonucci 1993) cannot be ruled out. These narrow components have Equivalent Widths (EW) typically as large as 100 eV, and may contribute as much as 50% to the total iron line flux (Weaver 2001).

In this context, we present in this paper X-ray observations of the Seyfert 1 galaxy ESO 198-G24 ($z = 0.0455$). Relatively little is known on its X-ray spectral properties, despite the fact that it belongs to the Piccinotti sample (H0235-52; Piccinotti et al. 1982), and hence it is one of the brightest AGN of the 2–10 keV sky. In their EXOSAT AGN survey paper, Turner & Pounds (1989) note that it exhibits a "canonical spectrum" (photon index, $\Gamma = 1.88\pm^{0.16}_{0.08}$) with "no significant low-energy absorption", and a 2–10 keV luminosity $\simeq 1.64 \times 10^{44}$ erg s^{-1}, about three times lower than during the HEAO-1 scans. In the ROSAT All-Sky Survey

Send offprint requests to: M. Guainazzi,
e-mail: mguainaz@xmm.vilspa.esa.es

(Schartel et al. 1997) a rather steeper soft spectral index was found ($\Gamma = 2.5 \pm 0.1$), again without any evidence for absorption. The 0.1–2.4 keV observed flux [$(5.33 \pm 0.13) \times 10^{-11}$ erg cm^{-2} s^{-1}] corresponds to a luminosity of $\simeq 2.0 \times 10^{44}$ erg s^{-1} once corrected for Galactic absorption ($N_{\rm H,Gal} = 3.2 \times 10^{20}$ cm^{-2}; Dickey & Lockman 1990) and extrapolated into the 2–10 keV band. Malizia et al. (1999) report a detection by BATSE, with a 2–100 keV flux of $(5.3 \pm 1.7) \times 10^{-11}$ erg cm^{-2} s^{-1}. To our knowledge, no result has ever been published from ASCA, BeppoSAX or XMM-Newton observations of this source so far.

This paper attempts to address this lack in the literature. The log of the observations presented in this paper is reported in Table 1, together with the corresponding exposure times and count rates in the energy bands where the spectral analysis discussed in Sect. 2 was carried out. The paper is organized as follows: Sect. 2 describes the spectral analysis, employing phenomenological models only. A comparison of the observed fluorescent iron K_α line profiles with the predictions of theoretical models is presented in Sect. 3. The results are discussed in Sect. 4. Throughout this paper: energies are quoted in the source reference frame; uncertainties are at the 90% confidence level for one interesting parameter; $H_0 = 50$ km s^{-1} Mpc^{-1} and $q_0 = 0.5$, unless otherwise specified.

2. Spectral results

2.1. XMM-Newton

In this paper only the time-averaged pn (Strüder et al. 2001) spectrum in the 2–15 keV band will be presented. No significant spectral variability is associated with a ±7% flux fluctuation observed during the XMM-Newton observation. The source was outside the MOS1 field of view. The MOS2 exposure was performed in Timing Mode. The calibration of this mode is still preliminary, and the corresponding data will not de discussed in this paper. The pn observation was performed in Small Window Mode with the blocking optical Medium filter. Data were reduced with SAS v5.3.3 (Jansen et al. 2001), using the most updated calibration files available as of July 1, 2002. A spectrum including single- and double-pixel events was extracted. It was verified that spectra extracted with either only single- or only double-pixel events are mutually consistent within the statistical uncertainties. Source spectra were extracted from a circular region of 1.8′ radius. Non X-ray background remained low throughout the observation, hence the whole integration time of the observation was used. Several recipes to extract the background spectra were compared, and yielded very similar results. The results presented in this paper were obtained with background spectra extracted from blank field templates available at the XMM-Newton Science Operation Center (Lumb et al. 2002), and rescaled in order to match the observed spectrum in the 15–20 keV energy band. The background contributes around 3% and 8% of the total spectrum at 2 and 5.5 keV respectively, and is brighter than the source above 10 keV. The spectra used throughout this paper were rebinned in such a way that: a) the intrinsic energy resolution of the detectors is sampled by a number of spectral channels not larger than 3; b) each spectral bin has at least 50 counts, to ensure the applicability of the χ^2 test. The same criteria were applied for the BeppoSAX and ASCA spectra discussed later, but the number of counts in these cases was limited to 25.

All the models discussed in this Section and in the following ones are modified by photoelectric absorption, whose column density, $N_{\rm H}$, is constrained to be not lower than the contribution due to the interstellar matter in our Galaxy along the line-of-sight to ESO 198-G24.

A simple power-law model is a marginally acceptable description of the pn spectrum ($\chi^2 = 146.5/114$ degrees of freedom, d.o.f.). A count excess around 6 keV (observer's frame) is present. The addition of a narrow (i.e. intrinsic width, σ, equal to 0) Gaussian emission profile to the best-fit power-law yields an improvement of the χ^2 by 18.3 for a decrease by 2 in the number of degrees of freedom (this quantity will be indicated as $\Delta\chi^2/\Delta\nu$ hereinafter), significant at the 99.992% confidence level. Leaving the intrinsic width of the Gaussian profile free in the fit yields a further improvement in its quality ($\Delta\chi^2/\Delta\nu = 5.8/1$, significant at the 98.8% confidence level). The best-fit parameters of the line are: $\sigma = 140\pm^{180}_{80}$ eV, centroid energy $E_{\rm c} = 6.43 \pm 0.07$ keV, and $EW = 180 \pm 70$ eV. The centroid energy is consistent with K_α fluorescence from neutral or mildly ionized iron, and strictly inconsistent with species more ionized than FeXIX. The intrinsic width is constrained to be larger than about 40 eV at the 90% confidence level for two interesting parameters (see Fig. 1). The upper limit is more loosely constrained, and widths as large as 0.5 keV are in principle possible.

The profile of the iron line may be more complex than a single broad Gaussian. A careful inspection of the residuals (see Fig. 2) suggests an additional emission feature with $E_{\rm c} \simeq 5.4$ keV (observer's frame). If an additional Gaussian profile is added to the model, the quality of the fit is improved at the 96.3% confidence level ($\Delta\chi^2/\Delta\nu = 9.3/3$). The best-fit values of this component are $E_{\rm c} = 5.70\pm^{0.07}_{0.12}$ keV, $EW = 70\pm40$ eV and $\sigma < 280$ eV. In order to compare its significance with the current systematic uncertainties of the pn response matrix, we analyzed pn public data of featureless calibration sources, acquired in Small Window Mode and reduced under the same conditions as the ESO 198-G24 data. Typical systematic uncertainties (represented by the shaded area in Fig. 3) are ±5% in the 5–7 keV band. We rule out therefore an instrumental origin for the $E_{\rm c} \simeq 5.7$ keV feature. Table 2 summarizes the spectral results.

The width of the $E_{\rm c} \simeq 6.4$ keV feature is not due to the presence of the additional line at $E_{\rm c} \simeq 5.7$ keV. If the data are fit with a model constituted by a power-law and one Gaussian profile, after removing the data points in the 5.0–5.5 keV energy range (observer's frame), the parameters of the Gaussian profile are: $E_{\rm c} = 6.43 \pm 0.08$ keV, $\sigma = 150\pm^{180}_{70}$ eV, $EW = 200\pm^{100}_{80}$ eV, therefore indistinguishable from those obtained with the complete model on the whole 2–15 keV energy band.

No further lines are statistically required by the fit. No evidence exists for photoelectric absorption edges in the pn spectrum either. The 90% upper limits on the optical depth of

Table 1. Log of the observations presented in this paper.

Mission	Observation date	Exposure time (ks)	Count rates (s^{-1})
ASCA (SIS0/GIS2)	July 10, 1997	31.1/34.3	0.153 ± 0.003/0.135 ± 0.002
XMM-Newton (pn/RGS1)	December 1, 2000	6.8/13.0	5.50 ± 0.03/0.184 ± 0.003
BeppoSAX (LECS/MECS/PDS)	January 23, 2001	55.1/143.3/51.3	0.1048 ± 0.0015/0.1723 ± 0.0011/0.32 ± 0.03

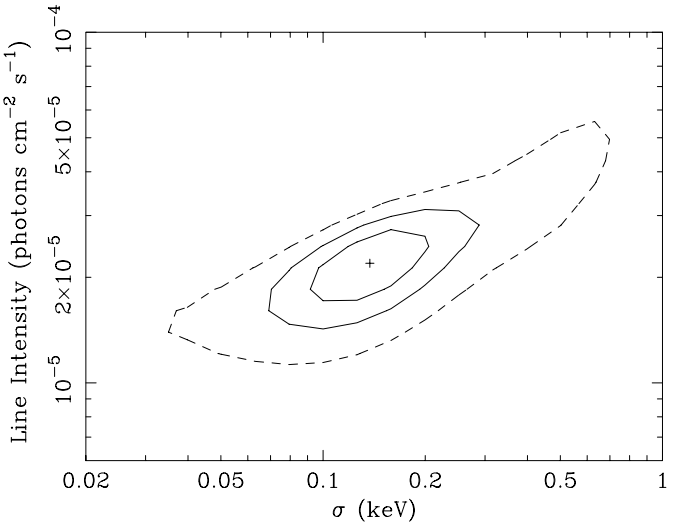

Fig. 1. Iso-χ^2 contours for the fluorescent iron K_α line intrinsic width (σ) versus intensity in the XMM-Newton observation of ESO 198-G24. Contours correspond to $\Delta\chi^2 = 1$, 2.71 (*solid lines*) and 4.61 (*dashed line*), respectively.

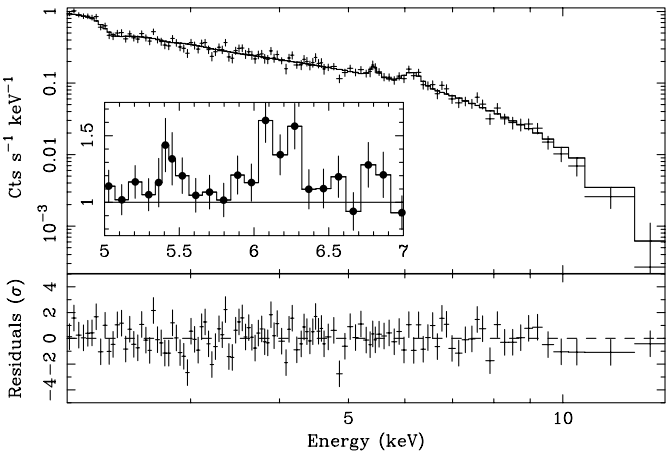

Fig. 2. Spectrum (*upper panel*) and residuals in units of standard deviations (*lower panel*) when the best-fit model as in Table 2 is applied to the pn data of ESO 198-G24. In the *inset*, the data/model ratio in the 5–7 keV energy range is shown, when the best-fit continuum is determined after the data points in the 5.0–6.5 keV (observer's frame) are removed.

un-blurred FeI, FeXXV and FeXXVI K edges are 0.14, 0.24 and 0.30, respectively.

2.2. ASCA

ASCA data were retrieved from the public HEASARC archive as screened event lists. Data reduction followed standard

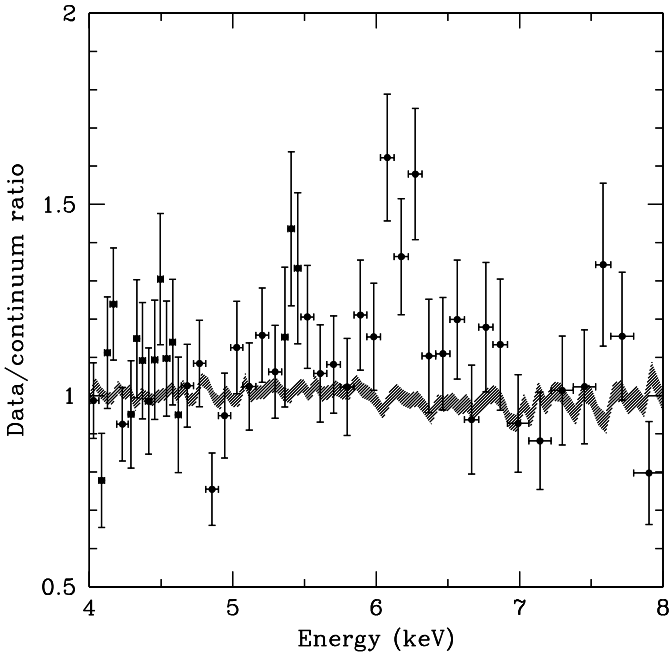

Fig. 3. Ratio of the ESO 198-G24 pn spectrum against the best-fit continuum model as in Table 2 (*filled circles*). The *shaded area* represents the $\pm1\sigma$ residuals against the best-fit 2–15 keV power-law model in an observation of the featureless AGN 3C273 (Obs. ID #0136550101 in revolution 277). They represent typical systematics associated with the pn response matrix employed in this paper.

procedures as described in, e.g., Guainazzi et al. (2000). Spectra of all the ASCA instruments were integrated on the whole elapsed time of the observation, after verifying that one can neglect spectral variability effects, and were simultaneously fit, allowing free normalization factors for the individual instruments to account for systematic uncertainties in the cross-normalizations (±7%). A simple power-law continuum modified by intervening photoelectric absorption yields a marginally acceptable fit to the data ($\chi^2 = 413.7/364$ d.o.f.). The 2–10 keV flux is about two times weaker than in the XMM-Newton observation. The residuals exhibit a clear narrow excess feature at about 6 keV (observer's frame). The addition of a narrow Gaussian profile largely improves the quality of the fit ($\Delta\chi^2/\Delta\nu = 28.7/2$, significant at the 99.9998% confidence level). The centroid energy is again consistent with neutral or mildly ionized iron ($E_c = 6.40\pm^{0.09}_{0.05}$). No additional improvement in the χ^2 is obtained if the line width is left free in the fit. The 90% upper limit on its σ is 50 eV only. Similarly, the inclusion of a further Gaussian emission profile with $E_c \simeq 5.7$ keV is not statistically required ($\Delta\chi^2/\Delta\nu = 4.2/3$).

Table 2. Best-fit parameters and results, when the iron line emission is modeled with a combination of Gaussian profiles. Continua are power-laws for the XMM-Newton and ASCA observations, and a power-law modified by Compton-reflection for the BeppoSAX observation. The subscripts "SG" and "DG" refers to the fit of the iron line profile with a single or a double Gaussian profile, respectively.

	BeppoSAX	XMM-Newton	ASCA
Continuum			
F_h[a]	15.04 ± 0.10	10.90 ± 0.11	5.91 ± 0.16
L_X[b]	6.85 ± 0.09	4.20 ± 0.09	2.01 ± 0.07
Γ	1.79 ± 0.04	1.77 ± 0.03	$1.75\pm^{0.05}_{0.03}$
$N_{H,int}$[c]	<0.5	≤3.2	≤13.2
"6.4 keV" feature			
E_c (keV)	6.4 ± 0.2	6.43 ± 0.07	$6.40\pm^{0.09}_{0.05}$
σ (eV)	300 ± 300	$140\pm^{120}_{70}$	$0\pm^{50}_{0}$
I[d]	$1.7\pm^{0.5}_{1.0}$	$2.3\pm^{1.2}_{0.7}$	$2.2\pm^{0.5}_{0.7}$
EW (keV)	$100\pm^{30}_{60}$	$190\pm^{100}_{60}$	$320\pm^{70}_{100}$
"5.7 keV" feature			
E_c (keV)	...	$5.70\pm^{0.07}_{0.12}$	...
σ (eV)	...	$0\pm^{280}_{0}$	...
I[d]	...	1.0 ± 0.5	...
EW (keV)	...	70 ± 40	...
$\chi^2_\nu\|_{SG}$	1.14	1.11	1.06
$\chi^2_\nu\|_{DG}$	...	1.06	...

[a] 2–10 keV observed flux in units of 10^{-12} erg cm^{-2} s^{-1}.
[b] Unabsorbed 0.1–100 keV luminosity in units of 10^{44} erg s^{-1}.
[c] Column density of the intrinsic (i.e. at $z = z_{ESO\ 198-G24}$) absorber in units of 10^{20} cm^{-2}.
[d] In units of 10^{-5} photons cm^{-2} s^{-1}.

A summary of the best-fit results is shown in Table 2. The ASCA spectra and corresponding best-fit model are shown in Fig. 4.

2.3. BeppoSAX

BeppoSAX data were retrieved from the A.S.I. BeppoSAX Science Data Center (ASDC) public archive. Spectra from the Low Energy Concentrator Spectrometer (LECS, 0.1–4 keV; Parmar et al. 1997) and the Medium Energy Concentrator Spectrometer (MECS, 1.8–10 keV; Boella et al. 1997) were extracted from linearized and calibrated event lists, following standard recipes as detailed in, e.g., Guainazzi et al. (1999). Background spectra were extracted from blank sky field event lists provided by the ASDC, using the same area in detector coordinates as the source. Extraction radius were 8′ and 4′ for the LECS and the MECS, respectively. Background-subtracted spectra for the Phoswitch Detector System (PDS, 13–200 keV; Frontera et al. 1997) were generated by plain subtraction of the 96 s duty-cycle intervals, when the collimators were pointing to the line of sight towards ESO 198-G24 and to a region 3.5° degrees aside. Spectra were integrated on the whole elapsed time of the observation, after verifying that one can neglect spectral variability effects, and were simultaneously fit after applying correction factors, to account for known differences in the absolute flux cross-calibration of the instruments (in particular, a value of 0.84 was employed for the PDS versus MECS normalization; Fiore et al. 1998).

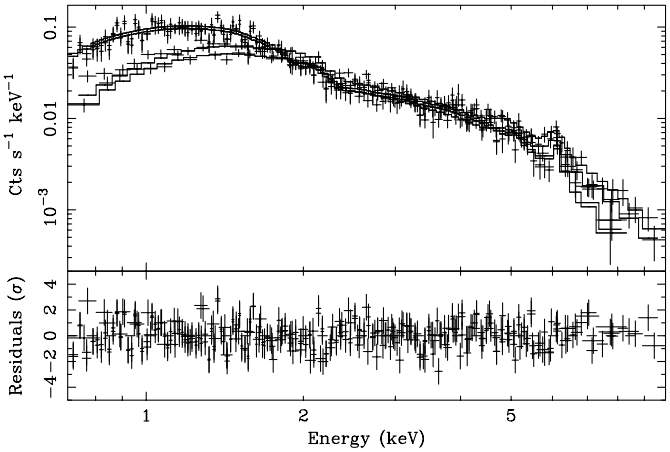

Fig. 4. Spectrum (*upper panel*) and residuals in units of standard deviations (*lower panel*) when the best-fit model as in Table 2 is applied to the ASCA data of ESO 198-G24.

A marginally acceptable fit (χ^2 = 170.3/144 d.o.f.) is obtained with the standard Seyfert 1 continuum model in the BeppoSAX energy bandpass (Perola et al. 2002), i.e., a photoelectrically absorbed power-law, modified by Compton-reflection from cold matter (Lightman & White 1988; George & Fabian 1991; Magdziarz & Zdziarski 1995). Assuming an inclination angle of the reprocessing matter $i = 25°$, R[1] is comprised between 0.1 and 1.0 at the 90% level for two interesting parameters (cf. the left panel of Fig. 5).

Any thermal cut-off in the intrinsic power-law is constrained to lay at energies $E_{cutoff} \gtrsim 150$ eV at the same confidence level (cf. the right panel of Fig. 5). The spectral index of the *intrinsic* power-law ($\Gamma = 1.79 \pm 0.04$) is remarkably close to the XMM-Newton and ASCA *observed* indices. The BeppoSAX best-fit parameters values are only marginally affected by different choices of the inclination angle, e.g.: R changes by 0.1 and Γ by 0.02 if $i = 45°$.

Excess residuals around $E \simeq 6$ keV (observer's frame) again suggest emission from a fluorescent iron K_α line. The addition of a Gaussian profile yields an improvement in the quality of the fit by $\Delta\chi^2/\Delta\nu = 8.5/3$, significant at the 93.5% confidence level. No conclusion can be drawn on the intrinsic width of the line profile. Its total EW does not exceed 130 eV. A summary of the best-fit results is shown in Table 2. The best-fit model and residuals are shown in Fig. 6.

3. The history of the iron line profile in ESO 198-G24

Table 2 summarizes the best-fit results for the ASCA, XMM-Newton and BeppoSAX observations of ESO 198-G24, when the iron line is fit by a (combination of) Gaussian profile(s). These observations span a range of about 3 in 2–10 keV X-ray flux, whereas the spectral shape of the continuum does not exhibit significant changes. Anecdotically, the ASCA observation

[1] R is proportional to the ratio between the normalizations of the reflected and of the primary continuum component. If the primary emission is isotropic, $R = \Omega/2\pi$, where Ω is the solid angle subtended by the reflector to the primary continuum source.

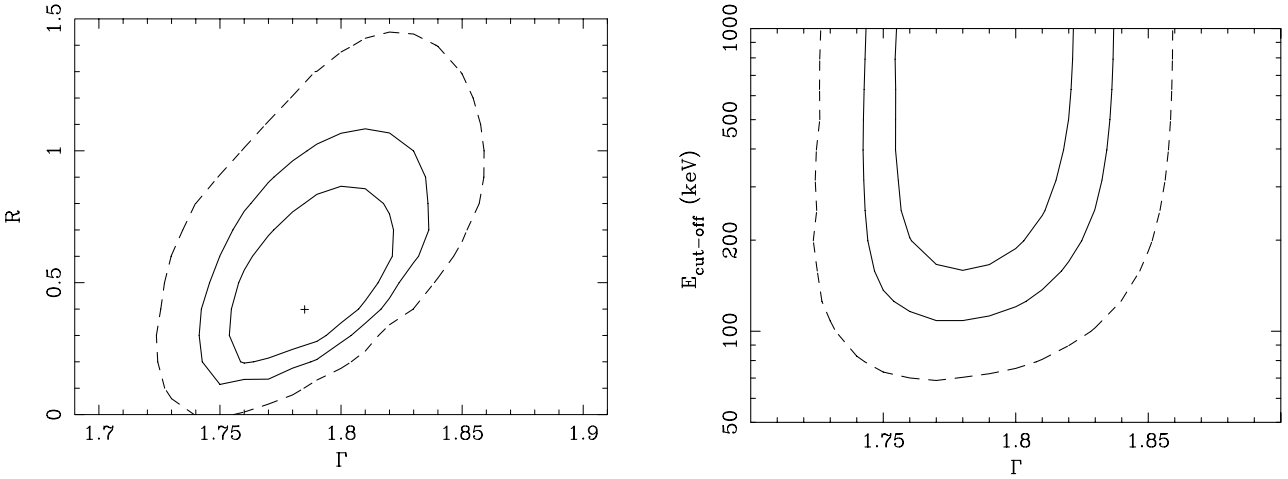

Fig. 5. Iso-χ^2 contour plots for the spectral index versus the Compton-reflection R parameter (*left panel*) and the high energy cut-off (*right panel*) for the BeppoSAX observation of ESO 198–G24. Contours correspond to the 68%, 90% (*solid lines*) and 99% (*dashed lines*) confidence levels for two interesting parameters, respectively.

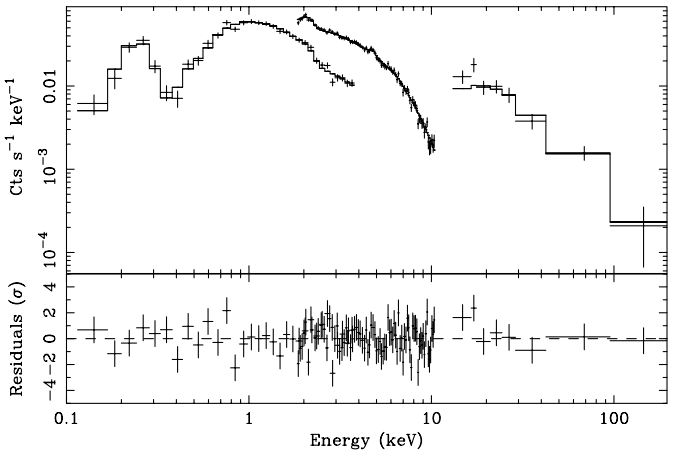

Fig. 6. Spectrum (*upper panel*) and residuals in units of standard deviations (*lower panel*) when the best-fit power-law plus Compton-reflection model is applied to the BeppoSAX data of ESO 198-G24. The line is accounted for by a single broad Gaussian profile.

caught ESO 198-G24 in its faintest state ever reported. Some of the properties of the iron line vary in a way, which is apparently correlated with the X-ray flux. The line *EW decreases* with increasing continuum flux, from $EW \simeq 320$ eV in the weakest (ASCA) to the $EW \simeq 100$ eV in the brightest (BeppoSAX) state. The narrow profile of the 6.4 keV emission line measured by ASCA ($\sigma < 50$ eV) is formally inconsistent with the broad profile measured by XMM-Newton ($\sigma \simeq 140$ eV). The centroid energy is always consistent with that of fluorescent transitions of neutral or mildly ionized iron. However, alternative interpretations are possible, when the line profile is significantly broadened or skewed.

Broad and asymmetric iron line profiles in AGN are naturally explained as due to relativistic effects, affecting the photons emitted in an X-ray illuminated accretion disk (Fabian et al. 1989; Laor 1991; Matt et al. 1992). If the line photons are emitted – originally with a monochromatic energy distribution – within a few gravitational radii from the source of an intense gravitational potential, the combination of kinematic (Doppler) and gravitational shifts over a range of disk annuli can produce significant broadening and skewing of the profile.

The iron line profile can be best studied in the pn spectrum, thanks to its combination of photon statistics and instrumental energy resolution. Bearing the above scenario in mind, the observed excess in the 5–6.5 keV (observer's frame) energy range was fit with relativistic emission line profiles, as expected around a Schwarzschild (model DISKLINE in XSPEC; Fabian et al. 1989) or a Kerr (model LAOR in XSPEC; Laor 1991) black hole. These models depend on a number of parameters: apart from the centroid energy and the normalization, the inner ($r_{\rm i}$) and outer ($r_{\rm o}$) radius of the line emitting region in units of Schwarzschild radii ($R_{\rm S}$), the inclination of the accretion disk (i), and the power-law of the radial emissivity dependence (q). The available statistics is not sufficient to allow all these parameters to be simultaneously constrained by the fit. The fits were therefore performed in two steps. In the first step, all the parameters were left free to vary, and their confidence intervals calculated to determine which of them are unconstrained. The unconstrained parameters were then frozen to physically plausible values and/or intervals in the second step. The final results are summarized in Table 3.

The comparison between the best-fit relativistic profiles and the data is shown in Fig. 7. Deviations between individual data points and the models are around $\pm 1\sigma$. Nonetheless, a description of the 5–6.5 keV (observer's frame) excess in terms of a double Gaussian profile is better than the single relativistic profile at the 94.6% (Schwarzschild) and 96.5% (Kerr) confidence level, respectively. The relativistic profiles exhibit complementary virtues and problems. The Schwarzschild profile follows better the overall excess shape, but remains slightly below the observed blue peak; the Kerr profile does not "see" the read peak, of course. Interestingly enough, both models rules out that the bulk of the photons are originally emitted by He- or H-like iron, as $E_{\rm c} \lesssim 6.6$ keV. The addition of a farther narrow line component underneath or besides the relativistically

Table 3. Best-fit results when the XMM-Newton/pn iron line profile is fit with a relativistic profile.

Observation	E_c (keV)	r_i (R_S)	r_o (R_S)	q	i (°)	EW (keV)	χ^2_ν
Schwarzschild profile	$6.40^{+0.17}$	$17\pm_{8}^{<r_o}$	$35^{+18}_{>r_i}$	-2^a	$25\pm_{7}^{3}$	$340\pm_{120}^{110}$	1.08
Kerr profile	$6.40^{+0.05}$	$8.2\pm_{7.0}^{5.0}$	$1700\pm_{800}^{1700}$	-3^a	<39	$280\pm_{760}^{110}$	1.09

[a] Unconstrained and therefore fixed in the fit to the reported value.

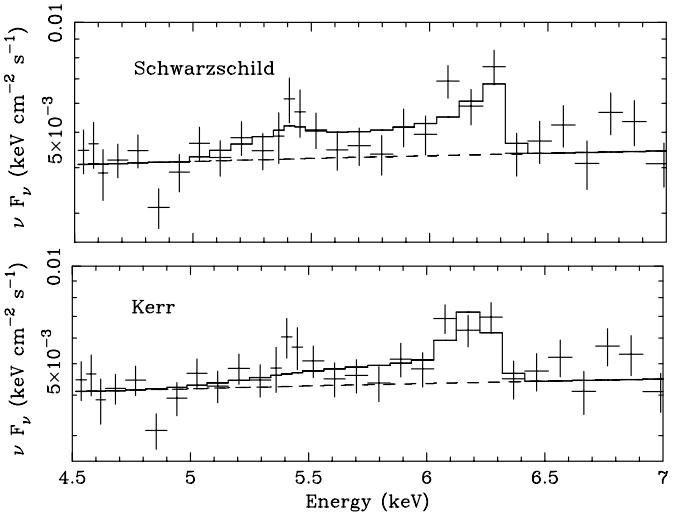

Fig. 7. Spectrum (*crosses*) and best-fit model in the 4.5–7 keV energy band, when the iron K_α emission line is modeled with a purely relativistic emission, around a Schwarzschild (*upper panel*) and Kerr (*lower panel*) black hole.

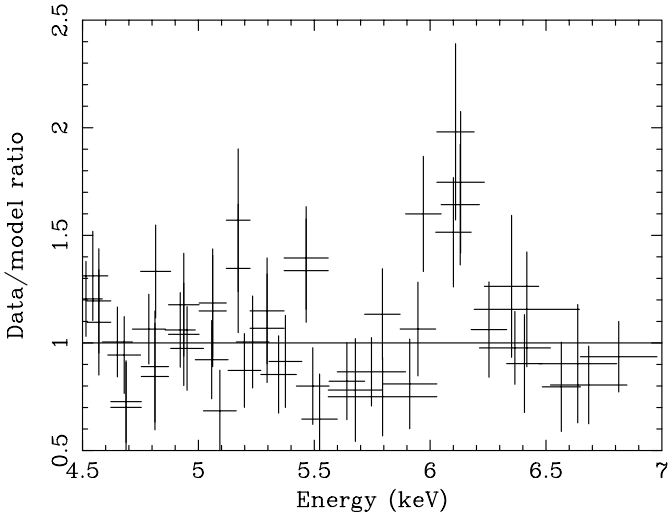

Fig. 8. Residuals (in data/model ratio) when a purely relativistic profile, with all its parameter (except the normalization) constrained within the best-fit XMM-Newton confidence intervals (cf. Table 3), is fit to the ASCA iron emission line.

broadened profile yields a negligible improvement in the quality of the fit ($\Delta\chi^2 \lesssim 2$), even if the centroid energy of the narrow component is fixed to the value corresponding to a fluorescent neutral iron K_α line.

Limited constraints can be derived on the iron line shape from either the ASCA or the BeppoSAX observation. The ASCA line is clearly narrow and no hint of a broad component exists. Nonetheless, the upper limits on the *EW* of an underlying relativistic profile, with the same shape as observed by XMM-Newton, are not particularly demanding: 720 eV and 300 eV for a Schwarzschild and a Kerr profile, respectively (cf. Fig. 8). In the BeppoSAX spectrum, due to the relative weakness of the iron line, and to the comparatively poorest energy resolution of the MECS detector, the question whether the line profile is broad or narrow remains basically unanswered.

4. Discussion

The history of the iron K_α line profile in ESO 198-G24 can be summarized as follows (in order of increasing 2–10 keV flux):

– in the ASCA observation the line profile is narrow, and no indication of a broad component is present;
– the XMM-Newton pn spectrum exhibits a broad line, centered at $E_c \simeq 6.4$ keV, alongside with a possible (confidence level: 96.3%) additional feature at $E_c \simeq 5.7$ keV. The latter feature does not correspond to any atomic transitions, and would therefore most likely belong to a relativistic profile together with the main "6.4 keV" component;
– in the BeppoSAX observation the line has an *EW* by a factor 2 (3) fainter than in XMM-Newton (ASCA). It is impossible to tell whether its profile is narrow or broad.

If the emission feature at $E_c \simeq 5.7$ keV detected in the pn spectrum indeed belongs to a relativistic profile, the iron line complex observed in ESO 198-G24 may be one example of "double-horned" profile. Unfortunately, the statistics in the rather short XMM-Newton observation is not good enough to allow an unambiguous description in terms of a specific relativistically broadened profile. Models employing the Schwarzschild or Kerr kernel can equally well describe it form the statistical point of view (although the latter does not have any red peaks!). Interestingly enough, the best description of the excess in the 5–6.5 keV energy range (observer's frame) is in terms of a combination of two Gaussians. The main reason for this is that the 5.7 keV and 6.4 keV features have comparable intensities (within a factor of 2), while keeping a separation $\Delta E/E \simeq 0.15$. They could hardly belong to a common standard single relativistic profile, because such a large relativistic broadening implies generally a much stronger blue peak (Fabian et al. 1989; Matt et al. 1991). Changes in the basic relativistic profile model, such as absorption by inner shell transitions of ionized iron (as proposed by Sako et al. 2002), or emission by a single "flare", which illuminates only a small fraction

of the disk surface (as proposed by Nayakshin & Kazanas 2001 and Yaqoob et al. 2001), do not yield any statistically significant improvements in the quality of the fit.

The *EW* of the line observed by BeppoSAX a few weeks later is by a factor of 2 weaker than measured by XMM-Newton, whereas the continuum flux was about 60% more intense. If the BeppoSAX profile is dominated by a broad component, this evidence suggests that the response time of the relativistic line to variations of the underlying continuum is probably larger than at least a few hours. If the solid angle subtended by the reprocessing matter and the spatial distribution of the intrinsic continuum did not change between the two observations (which is consistent with the closeness between the *intrinsic* spectral index measured by BeppoSAX and the *observed* spectral index measured by XMM-Newton), the larger *EW* of the relativistic profile in the pn spectrum can be explained by a delayed response to a brighter continuum flux state before the start of the pn exposure. The delay is at least of the order of the pn exposure elapsed time, i.e. $\gtrsim$2 hours, corresponding to a spatial scale of $\gtrsim 7 R_S M_8^{-1}$, if M_8 is the black hole mass in units of 10^8 solar masses. Fabian et al. (2002) point out similar problems to explain the short time scales variability pattern of the relativistic line in MCG-6-30-15. If the BeppoSAX profile is substantially "contaminated" by a narrow component, the discrepancy between the broad component *EW*s is obviously even larger.

By contrast, the ASCA line profile is dominated by a remarkably narrow "core". Unresolved iron lines have been now quite commonly discovered both in *Chandra* grating (Yaqoob et al. 2001; Kaspi et al. 2002) and in XMM-Newton observations (Gondoin et al. 2001a,b; Reeves et al. 2001; Petrucci et al. 2002; O'Brien et al. 2001). The two most plausible possibilities are Compton-reflection by matter far off the central engine (e.g., the "torus"), or gas clouds in the Broad Line Regions. The *EW* of the narrow line in ASCA ($\simeq$300 eV) is much larger than typically observed (50–100 eV). If it originates in the torus, one may expect $EW \simeq 100$ eV if the torus subtends a solid angle $\sim\pi$ (Krolik et al. 1994; Ghisellini et al. 1994). Such a large *EW* may be therefore indicative either of a strong (a factor $\gtrsim$10) iron overabundance or, more likely, of the "echo" of a brighter illuminating flux state. Our sparse knowledge of the historical X-ray light curve of ESO 198-G24 indeed suggests a dynamical range of at least a factor 6 in the nuclear power.

Acknowledgements. Comments by an anonymous referee strongly contributed to improve the quality of the presentation and sharpen the focus of this paper. This paper is based on observations obtained with XMM-Newton, an ESA science mission with instruments and contributions directly funded by ESA Member States and the USA (NASA). The XMM-Newton Science Archive (XSA) Development Team is gratefully acknowledged for its highly professional work. This research has made use of data obtained through the High Energy Astrophysics Science Archive Research Center Online Service, provided by the NASA/Goddard Space Flight Center and of the NASA/IPAC Extragalactic Database (NED) which is operated by the Jet Propulsion Laboratory, California Institute of Technology, under contract with the National Aeronautics and Space Administration.

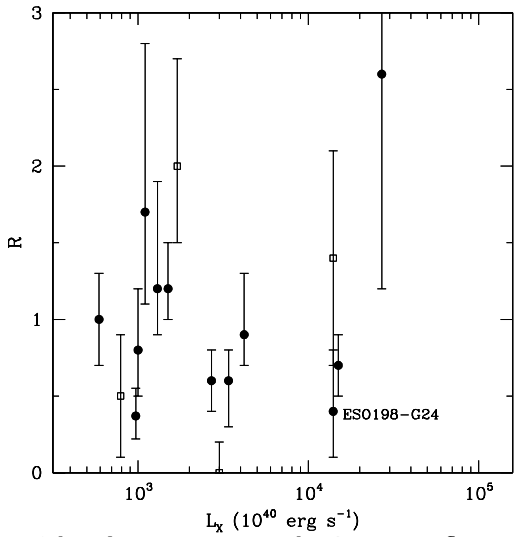

Fig. 9. 2–10 keV luminosity versus the Compton-reflection relative intensity *R* for a PDS count rate limited sample of publicly available type 1 (*filled circles*) and type 2 (*empty squares*) Seyferts observed by BeppoSAX.

Appendix: On the "X-ray Baldwin effect"

ESO 198-G24 is one of the brightest Seyfert 1s where a fluorescent iron K_α line and a Compton reflection continuum have been simultaneously measured. The amount of reflection (assuming an inclination angle as derived by the fit of the iron line in the pn spectrum with a Schwarzschild profile: $i = 25°$) is $R = 0.4^{0.4}_{0.3}$, about one-half the value expected if the reprocessing occurs in a plane-parallel, semi-infinite slab, and the primary emission is isotropic.

Nandra et al. (1997b) and Reeves & Turner (2000) discuss a possible "X-ray Baldwin effect", whereby the intensity of the reprocessing features decreases with increasing AGN X-ray luminosity due to a higher degree of ionization of the accretion disk, which smears the spectral contrast between the reflected and direct continua and shifts the iron line centroid either to intermediate ionization stages, where resonant scattering may cause a reduction in the line flux (Matt et al. 1993, 1996), or to fully ionized stages. In ESO 198-G24 there is no compelling evidence for high iron ionization stages to be responsible for the bulk of the line profile in any of the scenarios discussed in this paper. In order to test the dependence of the Compton reflection on the luminosity, we retrieved from the BeppoSAX public archive data for a sample of Seyfert galaxies (of both type 1 and 2), having a PDS count rate larger then 0.35 s^{-1} [2]. We analyzed these observation, applying the standard Seyfert spectral template, as described in Perola et al. (2002), eventually modified for intervening photoelectric absorption in type 2 objects. The reprocessor is assumed always neutral, and the inclination angle as in Sect. 3. The *R* versus 2–10 keV luminosity (L_X) plot is shown in Fig. 9. There is no evidence for any

[2] The sample includes: ESO 191-G55, Fairall 9, IC 4329A, MCG 5-23-16, MCG 6-30-15, MCG-8-11-11, Mkn 509, NGC 2110, NGC 3516, NGC 3783, NGC 4151, NGC 4593, NGC 5506, NGC 5548, NGC 526A, NGC 7469. Measurements for MCG 6-30-15 are taken from (Guainazzi et al. 1999), for NGC 4151 from (Schurch & Warwick 2002).

correlations between these quantities, across the 2.5 dex span in luminosity.

References

Antonucci, R. 1993, ARA&A, 31, 473
Antonucci, R. R. J., & Miller, J. S. 1985, ApJ, 297, 621
Ballantyne, D. R., Ross, R. R., & Fabian, A. C. 2001, MNRAS, 327, 10
Boella, G., Butler, R. C., Perola, G. C., et al. 1997, A&AS, 122, 299
Cappi, M., Matsuoka, M., Otani, C., & Leighly, K. M. 1998, PASJ, 50, 213
Dickey, J. M., & Lockman, F. J. 1990, ARA&A, 28, 215
Fabian, A. C., Rees, M. J., Stella, L., & White, N. E. MNRAS, 238, 729
Fabian, A. C., Vaughan, S., Nandra, K., et al. 2002, MNRAS, 335, L1
Fiore, F., Guainazzi, M., & Grandi, P. 1998, Cookbook of BeppoSAX data analysis (BeppoSAX SDC: Roma)
Frontera, F., Costa, E., dal Fiume, D., et al. 1997, A&AS, 122, 347
George, I. M., & Fabian, A. C. 1991, MNRAS, 249, 352
Ghisellini, G., Haardt, F., & Matt, G. 1994, MNRAS, 267, 743
Gondoin, P., Lumb, D., Siddiqui, H., Guainazzi, M., & Schartel, N. 2001, A&A, 373, 805
Gondoin, P., Barr, P., Lumb, D., et al. 2001, A&A, 378, 806
Grandi, P., Guainazzi, M., Mineo, T., et al. 1997, A&A, 325, L17
Guainazzi, M., Dennefeld, M., Piro, L., et al. 2000, A&A, 335, 113
Guainazzi, M., Matt, G., Molendi, S., et al. 1999, A&A, 341, L27
Guainazzi, M., Perola, G. C., Matt, G., et al. 1999, A&A, 346, 407
Kaspi, S., Brandt, W. N., George, I. M., et al. 2002, ApJ, 574, 643
Krolik, J. H., Madau, P., & Życki, P. T. 1994, ApJ, 420, L57
Jansen, F., Lumb, D., Altieri, B., et al. 2001, A&A, 365, L1
Laor, A. 1991, ApJ, 376, 90
Lightman, A. P., & White, T. R. 1988, ApJ, 335, 57
Lumb, D. H., Warwick, R. S., Page, M., & De Luca, A. 2002, A&A, 389, L93
Magdziarz, P., & Zdziarski, A. A. 1995, MNRAS, 273, 837
Malizia, A., Bassani, L., Stephen, J. B., Malaguti, G., & Palumbo, G. C. C. 1997, ApJS, 113, 331
Matt, G., Brandt, W. N., & Fabian, A. C. 1996, MNRAS, 280, 823
Matt, G., Fabian, A. C., & Ross, R. R. 1993, MNRAS, 261, 346
Matt, G., Fabian, A. C., Guainazzi, M., et al. 2000, MNRAS, 318, 173
Matt, G., Guainazzi, M., Perola, G. C., et al. 2001, A&A, 377, L31
Matt, G., Perola, G. C., & Piro, L. 1991, A&A, 247, 25
Matt, G., Perola, G. C., Piro, L., & Stella, L. 1992, A&A, 257, 63
Nandra, K., George, I. M., Mushotzky, R. F., Turner, T. J., & Yaqoob, T. 1997, ApJ, 467, 70
Nandra, K., George, I. M., Mushotzky, R. F., Turner, T. J., & Yaqoob, T. 1997b, ApJ, L91
Nandra, K., George, I. M., Mushotzky, R. F., Turner, T. J., & Yaqoob, T. 1999, ApJ, 523, L17
Nandra, K., & Pounds, K. A. 1994, MNRAS, 268, 405
Nayakshin, S., Kazanas, D., & Kallman, T. R. 2000, ApJ, 537, 833
Nayakshin, S., & Kazanas, D. 2001, ApJ, 533, L141
O'Brien, P., Page, K., Reeves, J. N., et al. 2001, MNRAS, 327, L37
Parmar, A. N., Martin, D. D. E., Bavdaz, M., et al. 1997, A&AS, 122, 309
Perola, G. C., Matt, G., Cappi, M., et al. 2002, A&A, 389, 202
Petrucci, P. O., Henri, G., Maraschi, L., et al. 2002, A&A, 388, L5
Piccinotti, G., Mushotzky, R. F., Boldt, E. A., et al. 1982, ApJ, 253, 485
Pounds, K. A., Nandra, K., Stewart, G. C., George, I. M., & Fabian, A. C. 1990, Nature, 344, 132
Pounds, K., Reeves, J., O'Brien, P., et al. 2001, ApJ, 559, 181
Reeves, J. N., & Turner, M. J. L. 2000, MNRAS, 316, 234
Reeves, J. N., Turner, M. J. L., Pounds, K., et al. 2001, A&A, 365, L134
Sako, M., Kahn, S. M., Branduardi-Raymont, G., et al., submitted [astroph/0112436]
Schartel, N., Schmidt, M., Fink, H. H., Hasinger, G., & Trümper, J. 1997, A&A, 320, 696
Schurch, N. J., & Warwick, R. S. 2002, MNRAS, 335, 241
Strüder, L., Briel, U., Dannerl, K., et al. 2001, A&A, 365, L18
Tanaka, Y., Nandra, K., Fabian, A. C., et al. 1995, Nature, 375, 659
Turner, T. J., George, I. M., Nandra, K., & Mushotzky, R. F. 1997, ApJS, 113, 23
Turner, T. J., Mushotzky, R. F., Yaqoob, T., et al. 2002, ApJ, 574, L123
Turner, T. J., & Pounds, K. 1989, MNRAS, 240, 833
Ueno, S., Mushotzky, R. F., Koyama, K., et al. 1994, PASJ, 46, L71
Weaver, K. 2001, ASP Conf. Ser., 249, 389
Wilms, J., Reynolds, C. S., Begelman, M. C., et al. 2001, MNRAS, 328, L27
Yaqoob, T., George, I. M., Nandra, K., et al. 2001, ApJ, 546, 759